Directed chaotic transport in the tokamap with mixed phase space

A. B. Schelin and K. H. Spatschek

Institut für Theoretische Physik, Heinrich-Heine-Universität Düsseldorf, D-40225 Düsseldorf, Germany
(Received 8 October 2009; published 12 January 2010)

On the basis of the tokamap, characteristic features of magnetic field lines and zeroth-order guiding-center particle motion in the whole body of a magnetically confined plasma, e.g., a tokamak plasma, are investigated. It is shown that the tokamap exhibits a poloidal transport that can be considered as a Hamiltonian ratchet. In a situation with partially chaotic magnetic field lines the locking of the averaged poloidal velocity occurs to a value that does not depend precisely on the initial conditions. The so-called sum rule predicts the mean velocity in agreement with the observed magnitude. Possible consequences for the onset of poloidal plasma rotation in ergodized plasmas are elucidated.

I. INTRODUCTION

Transport in stochastic plasmas is a basic problem in classical statistical physics with important implications for nuclear fusion research [1]. It is widely agreed that anomalous, fluctuation-induced transport is one of the most challenging issues in tokamak and stellarator physics as well as plasma astrophysics and related areas. In laboratory plasmas, the principally phenomena of nonlinear transport are often overshadowed by the complexity of the device such as toroidal geometry, arrangements and shapes of the confining magnetic field coils, plasma-wall interaction, and so on. The underlying fluctuations may have different sources. Time-dependent magnetic fluctuations may be attributed to magnetohydrodynamic activities. Driftlike instabilities could result in predominantly electrostatic perturbations. Hardly any of the self-generated fluctuations can be analyzed with the simplest nonlinear theory, i.e., quasilinear theory, because of large amplitudes, existence of islands, and so on. As a consequence, anomalous transport theory is barely tapped both in laboratory and in astrophysical plasmas. Advanced purely numerical simulations lead not only to perceptions but also to a tremendous collection of data which, in many cases, still await analytical interpretation.

Recently, magnetic fluctuations have been triggered in tokamaks in a controlled manner. The magnetic fluctuations are produced by additionally installed external magnetic field coils. Although arising from a deterministic procedure, Hamiltonian chaos theory implicates stochasticity of the field line motion. Incomplete stochastization of the plasma edge may occur (see, e.g., Refs. [2–4] and references therein). That manipulation is now common in several tokamaks and may be even advantageous to avoid some of the most dangerous plasma phenomena. The theory of fluctuation-induced transport in externally generated deterministic chaotic magnetic field systems requires a thorough analysis of the coil arrangements, the calculation of the radial variation in toroidal Fourier modes of the magnetic fluctuations, and so on. This can, and has been accomplished. In general the formulations become algebraically complicated. In such a situation it will be advantageous to first consider only a few Fourier modes and to investigate the transport scenario independent of the details of the geometry, boundary conditions, opera-tional scenarios, and so on. Such a strategy leads to fundamental investigations based on elementary models. The advantages of comprehensible and qualitatively correct results, however, are being paid in part by the lack of usability for detailed quantitative analysis. The latter is not in the center of interest of the simple models being employed here.

Twist maps belong to the simplest approaches for the first insight into magnetic field line transport. We will use the tokamap, which has been proposed by Balescu and co-workers [5] to analyze magnetic field line and zeroth-order guiding-center particle motion in the whole body of a simple model for a tokamak plasma [6–8]. The tokamak has been anticipated already for interpreting several plasma phenomena such as transport barriers, reconnection, edge localized modes (ELMS), plasma rotation, and so on [7,8]. Toroidal rotation [9,10] is beyond the scope of the tokamap which provides Poincaré plots in the poloidal plane. Radial transport was investigated already [7,8] with results stimulated by the fact that the radial diffusion coefficient is space dependent. Here we concentrate on the angular (poloidal) transport. We shall analyze directed velocities in angular (poloidal) direction. For that we shall first use the "original" tokamap [5]. The results will have direct application to field line motion. Particle motion consists of copassing and counterpassing particles with respect to the magnetic field lines. For counterpassing particles we use the backward tokamap which results from the tokamap by reversing the direction of magnetic-field lines. Note that the backward tokamap is not identical to the inverse tokamap. Such an asymmetry may be typical for particle motion in a plasma (remember the different drift surfaces for codrifting and counterdrifting particles). The difference between any average velocity of comoving particles to the average velocity of countermoving particles will be attributed to an effective plasma rotation. The latter is being influenced by the degree of stochastization, as has been observed in experiments [9,11–18].

Recent advances in nonequilibrium statistical mechanics shed light on the generation of currents in stochastic systems. The ratchet effect, i.e., the generation of transport with a preferential direction [19], in systems with mixed phase space is now widely discussed [20–26]. Stochastic ratchets gave rise to an understanding of transport phenomena far from thermal equilibrium [19]. The generic model of a stochastic ratchet consists of a sawtooth potential with a noisy

driving. The potential, while being periodic, must be spatially asymmetric, and the noise should result from nonequilibrium situations. When the noisy driving is replaced by a purely deterministic one, one applies the notion deterministic ratchet [21,22,27–31]. Purely Hamiltonian dynamics with both regular and chaotic phase space structures or with complete chaos may cause Hamiltonian ratchets.

One of the first applications of ratchet currents was discussed in intracellular transport; meanwhile many more applications are evident in various areas, from nanotechnology [32] to plasma physics. In the latter field, the ponderomotive ratchet in a uniform magnetic field [33] and the impurity pinch in tokamak plasmas [34,35] were discussed. A ratchet-type average velocity was demonstrated for test particles moving *radially* in a stochastic potential when the magnetic field is space dependent [34]. This constitutes a possible explanation for impurity behavior in tokamak plasmas [35]. Impurity control in magnetically confined plasmas is a very important issue for the development of fusion reactors. The experimental results show the accumulation of the impurities in the central region of the plasma, which appears to be a directed transport (a pinch) rather than a diffusive one. In the present paper we shall investigate whether the tokamap also allows for a directed chaotic transport in the poloidal direction.

The tokamap, as well as its variants [34,36,47,38,39] and generalizations [40–44], can be assigned to a Hamiltonian H (see Appendix A). The kinetic energy is positive definite, but has a generalized form compared to the standard one. Checking the tokamap against other (simple) models, e.g., the kicked rotator and its variants such as the standard map [45], the potential energy is significantly different. The amplitude of the periodic potential is momentum-dependent. That behavior is typical for plasma maps modeling toroidal systems. Thus, we have a type of potential which has not yet investigated in view of directed chaotic transport via a Hamiltonian ratchet process. Directed chaotic poloidal transport, if it occurs, may have an interesting consequence for the interpretation of poloidal rotation in ergodized plasmas.

The paper is organized as follows. In Sec. II we start with a brief summary of the tokamap model and its variants. Section III presents the results from numerical evaluations of the tokamap. The findings are interpreted in Sec. IV by the so-called sum formula. Implications on the plasma rotation are discussed in Sec. V. The manuscript is concluded by a short summary and conclusion. Appendix A deals with specific aspects of the tokamap. Predictions of the sum formula will be tested also for the bounded tokamap in Appendix B.

II. MODEL

A. Basic definitions and notation

A large class of area-preserving one-degree-of-freedom ($N=1$) maps can be cast in the form [47] $x_{k+1}=x_k+\Omega(y_{k+1})+f(x_k,y_{k+1})$ and $y_{k+1}=y_k+g(x_k,y_{k+1})$. The area-preserving condition means that the Jacobian of the transformation of variables at "time" k to variables at time $k+1$ must equal unity, i.e., $J\equiv\left|\frac{\partial x_{k+1}}{\partial x_k}\frac{\partial y_{k+1}}{\partial y_k}-\frac{\partial y_{k+1}}{\partial x_k}\frac{\partial x_{k+1}}{\partial y_k}\right|=1$. Since $N=1$, this also

implies that the map is symplectic [48]. In the present case we get the condition $\frac{\partial f}{\partial x_k}+\frac{\partial g}{\partial y_{k+1}}=0$. That restriction can be easily fulfilled when we postulate $f(x_k,y_{k+1})=L\eta(x_k)h'(y_{k+1})$ and $g(x_k,y_{k+1})=-L\eta'(x_k)h(y_{k+1})$, where the prime denotes the derivative with respect to the argument. L is the control parameter.

The area-preserving condition can be also viewed from the point of view of canonical transformations. Provided we have a generating function of the form $F(x_k,y_{k+1})=x_ky_{k+1}+F_0(y_{k+1})+L\delta F(x_k,y_{k+1})$, which depends on the old coordinates x_k and the new momenta y_{k+1}. Then the transformation equations are $y_k=\frac{\partial F}{\partial x_k}$ and $x_{k+1}=\frac{\partial F}{\partial y_{k+1}}$, resulting in

$$x_{k+1}=x_k+\frac{\partial F_0}{\partial y_{k+1}}+L\frac{\partial\delta F}{\partial y_{k+1}}, \qquad (1)$$

$$y_{k+1}=y_k-L\frac{\partial\delta F}{\partial x_k}. \qquad (2)$$

With $\delta F=\eta(x_k)h(y_{k+1})$ symplecticity follows.

For twist maps, the angle x should vary monotonously with flux y, $\frac{\partial x_{k+1}}{\partial y_k}\neq 0$. That twist condition is a crucial assumption in the proofs of important theorems, e.g., the standard proof of the Kolmogorov-Arnold-Moser (KAM) theorem [46].

During the last decades, with respect to nondissipative systems, two symplectic maps attracted the interest of the broad physics community. The standard map, also called the Taylor-Greene-Chrikov map in some of the older literature [45,48,49], occurs (sometimes written with $\theta_k\equiv x_k$ and $p_k\equiv y_k$) for $\Omega(y)=y$, $\eta(x)=\cos(x)$, and $h(y)=1$, i.e., $F_0=\frac{1}{2}y_{k+1}^2$ and $\delta F=\cos(x_k)$, in the form $x_{k+1}=x_k+y_{k+1}$ and $y_{k+1}=y_k+L\sin(x_k)$. It has proven to be a very convenient model for the study of the typical behavior of Hamiltonian systems that yield a two-dimensional map. Here we have written the first equation without modulo 2π so that we have an area-preserving twist map ($\frac{\partial x_{k+1}}{\partial y_k}=1$). On the other hand, one of the simplest area-preserving nontwist maps is obtained [46] for $F_0=a(y_{k+1}-\frac{y_{k+1}^p}{p+1})$ and $\delta F=-\frac{b}{L}\cos(x_k)$, in the form $x_{k+1}=x_k+a(1-y_{k+1}^p)$ and $y_{k+1}=y_k-b\sin(x_k)$, where a and b are real numbers, $p>1$ is a positive integer (e.g., $p=2$) and $x\in(-\frac{1}{2},\frac{1}{2})$ mod 1. There are several ways to violate the twist condition; here $\frac{\partial x_{k+1}}{\partial y_k}=0$ at a single value of y.

For applications in nuclear fusion research, these two maps have the disadvantage that they do not apply to toroidal systems. That is the reason why other maps came into the focus of plasma physicists.

B. Tokamap and its variants

In magnetic confinement physics, toroidicity plays a key role. In toroidal configurations one may present $x\triangleq\vartheta$ as the poloidal angle coordinate and $y\triangleq\psi\sim r^2\sim\rho^2$ as the toroidal flux. Here, $\rho\sim r$ is the radial coordinate in the torus. More details are shown in Fig. 1. With the coordinates $\rho,\vartheta,\Phi\sim\varphi$ the torus (tokamak) is said to be described in cylindrical approximation. The tokamap and its variants can be considered as iterative symplectic maps with generating functions of the form
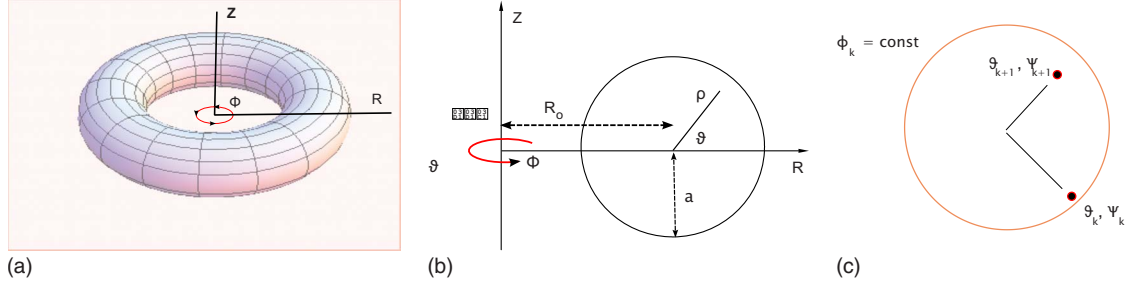
FIG. 1. (Color online) Geometry and coordinates relevant for the tokamap. From left to right: cylindrical coordinates R, Φ, and Z are used for the torus of a tokamak. Within a poloidal cross section the intrinsic coordinates ρ and ϑ are thenew plane polar coordinates. The mapping is within a certain poloidal cross section at constant azimuthal angle $\Phi \sim \varphi$ with $\psi \sim \rho^2$.

$$F(\vartheta_k, \psi_{k+1}) = \vartheta_k \psi_{k+1} + F_0(\psi_{k+1}) + L\delta F(\vartheta_k, \psi_{k+1}), \quad (3)$$

where $\delta F(\vartheta_k, \psi_{k+1}) = h(\psi_{k+1})\cos \vartheta_k$. The mapping follows as

$$\psi_k = \psi_{k+1} + L\frac{\partial \delta F(\psi_{k+1}, \vartheta_k)}{\partial \vartheta_k}, \quad (4)$$

$$\vartheta_{k+1} = \vartheta_k + 2\pi\Omega(\psi_{k+1}) + L\frac{\partial \delta F(\psi_{k+1}, \vartheta_k)}{\partial \psi_{k+1}}. \quad (5)$$

$\Omega(y_{k+1}) \equiv \frac{1}{2\pi}\frac{\partial F_0}{\partial y_{k+1}}$ is called the winding function.

The "original" tokamap, being compatible with the toroidal geometry, has been proposed by Balescu *et al.* [5] Compatibility with toroidal geometry means that the radial coordinate ψ should be positive definite. If $\psi_0 > 0$ at time zero, then at later "times" k we also should have $\psi_k > 0$. If $\psi_0 = 0$, then $\psi_k = 0$ should also hold. The tokamap follows from

$$F_0 = 2\pi\left[\psi_{k+1} - \frac{3}{4}\psi_{k+1}^2 + \frac{1}{3}\psi_{k+1}^3 - \frac{1}{16}\psi_{k+1}^4\right], \quad (6)$$

$$\delta F = -\frac{\psi_{k+1}}{1 + \psi_{k+1}}\cos(\vartheta_k). \quad (7)$$

Note that the winding number is

$$\Omega \equiv \frac{1}{q} \equiv \frac{\iota}{2\pi} = \frac{1}{4}(2 - \psi_{k+1})(2 - 2\psi_{k+1} + \psi_{k+1}^2), \quad (8)$$

The safety factor q was assumed as 1 at the center (magnetic axis), i.e., $q(0) = 1$. At the plasma edge $\psi = 1$, and q takes four times the central value, $q(1) = 4q(0)$. The function $q(\psi)$ is a monotonously increasing function of ψ. Summarizing, the tokamap is

$$\psi_{k+1} = \psi_k - L\frac{\psi_{k+1}}{1 + \psi_{k+1}}\sin(\vartheta_k), \quad (9)$$

$$\vartheta_{k+1} = \vartheta_k + 2\pi\Omega(\psi_{k+1}) - L\frac{1}{(1 + \psi_{k+1})^2}\cos(\vartheta_k). \quad (10)$$

Compared to the formulation in Ref. [7] $\vartheta = 2\pi\theta$ and $\Omega \equiv W$ holds. The original paper [5] uses in addition $K = 2\pi L$. In Appendix A, we present the Hamiltonian related to this map.

For reasons to become evident later we call the map (9)

and (10) the *forward tokamap*. The forward tokamap is an implicit map. However, the first equation (9) can be explicitly resolved with respect to ψ_{k+1},

$$\psi_{k+1} = \frac{1}{2}[\sqrt{P^2(\psi_k, \vartheta_k) + 4\psi_k} - P(\psi_k, \vartheta_k)], \quad (11)$$

where $P(\psi_k, \vartheta_k) = 1 - \psi_k + L\sin(\vartheta_k)$. From here we recognize that the condition that for $\psi_0 = 0$ also $\psi_k = 0$ should follow (invariance of the magnetic axis) will be violated for $L\sin(\vartheta_k) < -1$. As a consequence, in the tokamap global chaos appears for $L > 1$ [38]. We come back to this point when discussing the bounded tokamap.

The tokamap describes magnetic field line propagation and/or zeroth-order guiding-center particle motion in field-line direction (copassing particles). The magnetic-field perturbations follow from [50–52]

$$\frac{\delta B_\vartheta}{B_0} = L\frac{\rho \epsilon_T}{aH}\frac{\partial \delta F(\vartheta, \psi)}{\partial \psi}, \quad (12)$$

$$\frac{\delta B_\rho}{B_0} = -L\frac{a\epsilon_T}{\rho H}\frac{\partial \delta F(\vartheta, \psi)}{\partial \vartheta}, \quad (13)$$

where $\epsilon_T = a/R_0$ is the inverse aspect ratio, a being the minor radius, and R_0 the large radius of the torus. B_0 is the magnetic-field strength on the axis, and $H = 1 + \epsilon_T \frac{\rho}{a}\cos \vartheta$. The physical derivation of the tokamap suggests to introduce for particles moving in opposite direction to the magnetic field lines (counterpassing particles) the *backward tokamap* by changing $\Omega \rightarrow -\Omega$ and $L \rightarrow -L$,

$$\psi_{k+1} = \psi_k + L\frac{\psi_{k+1}}{1 + \psi_{k+1}}\sin(\vartheta_k), \quad (14)$$

$$\vartheta_{k+1} = \vartheta_k - 2\pi\Omega(\psi_{k+1}) + L\frac{1}{(1 + \psi_{k+1})^2}\cos(\vartheta_k). \quad (15)$$

The backward tokamap has the same structure as the forward tokamap; it is not identical with the inverse tokamap.

Summarizing this part one can understand the tokamap as the paradigm for global magnetic-field propagation in a tokamak. However, for quantitative results many more details have to incorporate into the symplectic twist map. Generalized maps [40–42] which recover all the details of the vacuum magnetic field topology of edge stochastization, e.g.,
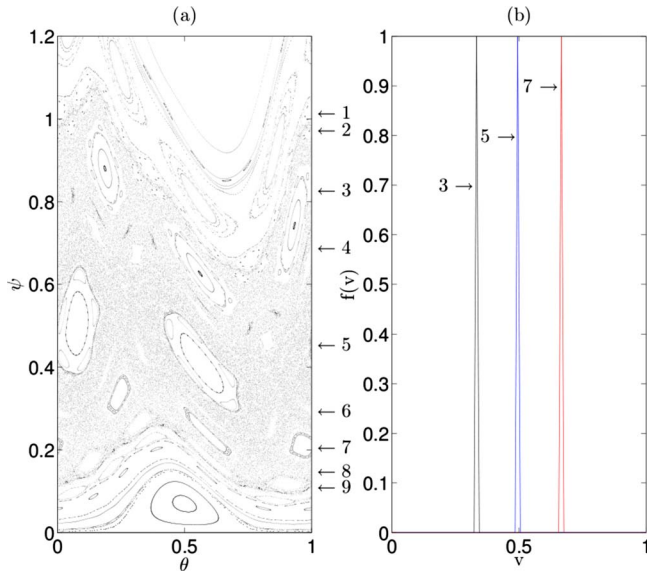
FIG. 2. (Color online) (a) Phase space of the tokamap for $L = 4.5/2\pi$. (b) Distribution of time-averaged velocities for the chains of islands 3, 5, and 7.

FIG. 3. (Color online) Distribution of time-averaged velocities in the chaotic sea at (a) $t \sim 10^3$, (b) $t \sim 10^4$, (c) $t \sim 10^5$ and (d) $t \sim 10^6$. As $t \to \infty$ it evolves to a narrow peak around the asymptotic velocity, $\overline{v_\theta} \approx 0.50 \pm 0.02$. We have $L = 4.5/2\pi$.

as occurring during the dynamic ergodic divertor (DED) operation at the tokamak TEXTOR, were developed. It was also recognized that besides magnetic-field-line motion, also the Hamiltonian for drift motion can be used as a starting point for very detailed studies of particle motion in stochastic tokamaks plasmas. Numerical results for poloidal plasma rotation were obtained [43,44]. The present paper is related to the latter investigations by exploring the principles of generating directed poloidal motion in stochastic plasmas.

In what follows we shall study first the poloidal field-line motion in the tokamaks (9) and (10). Then we shall have a short look at the backward tokamap in order to explore the possibility of plasma (particle) rotation.

III. POLOIDAL RATCHET CURRENT IN THE TOKAMAP

To describe the transport properties of the tokamap, we use velocity distributions of ensemble of initial positions (in the following called particles). The velocity is in the angular (poloidal) direction and, for each initial position θ_0, is given by

$$v = \frac{\theta_t - \theta_0}{t}, \tag{16}$$

where $\theta = \vartheta/2\pi$, and $t \sim k$ is the time. When we assume that real particles follow exactly the magnetic-field lines, without any collisions, θ_t corresponds to the position of a copassing (real) particle.

We first consider the forward tokamap [Eqs. (9) and (10)]. The phase portrait of the tokamap has already been fully described in [5]. Here, we set the stochastic parameter to $L = 4.5/2\pi$. For this parameter value, the map contains a mixed phase space: large island chains coexist with a stochastic sea and these are bounded, from below and above, by KAM surfaces [see Fig. 2(a)].

The different invariant sets of the phase space render different types of motion. Particles with initial positions inside islands display a regular motion with a well defined periodicity. In contrast, trajectories of the chaotic sea own a very complicated dynamics and, due to ergodicity, fill equally the stochastic region.

This affects the velocity distributions of an ensemble of particles. Take, for example, a group of particles distributed inside an island. The average (poloidal) velocity of this ensemble will be equal to the winding number of the island chain, ω. Figure 2(b) shows examples of such a case, where we plot the velocity distributions of ensembles inside three different island chains. For a distribution within the chaotic sea the behavior is alike. Most particles will also share the same mean velocity. This, however, only occurs after a long period of time, as we can see in Fig. 3, where the velocity distribution is shown for different time scales.

For the calculation of Fig. 3, we follow the method described by Schanz *et al.* [20]. We choose the ensemble of particles by running one chaotic trajectory that fills the chaotic sea; each point of this trajectory, then, is used as a new initial condition. For each initial condition, we calculate (16) at a fixed time t. This provides the probability distribution $f(v)$.

In order to understand Fig. 3, we now go back to individual orbits. Regular islands are impermeable to chaotic trajectories. In spite of this, they still have great influence on the dynamics of the chaotic region. There is a complex boundary between the chaotic sea and regular islands, composed by a set of barriers (cantori). Because of the barriers, a chaotic trajectory close to an island spends a long time following it, sharing also the same poloidal velocity.

This stickiness is reflected on the velocity distributions of chaotic trajectories. For $t \sim 10^3$ [Fig. 3(a)], $f(v)$ has many

peaks due to groups of particles following different islands. As time evolves, each particle eventually overcomes the stickiness and leaves, moving around the chaotic sea, until it is trapped by another island. Since the system is bounded, particles in the chaotic sea are destined to wander between the different island chains of the layer. After an amount of time t_f (for the forward tokamap $t_f \sim 10^5$), most particles will have visited all islands and, thus, the distribution $f(v)$ will resume to a narrow peak around the velocity $\overline{v_\theta}$ [Fig. 3(d)]. This velocity is, naturally, independent of initial conditions.

According to the definition proposed in Ref. [20], a Hamiltonian ratchet current exists when transport is ballistic, while spreading is not. There should be a locking of the average velocity to a specific, nonzero value that does not depend on initial conditions. As this is the case for the ensemble of chaotic trajectories, we argue here that the poloidal motion of particles in the tokamap can be regarded as a ratchetlike transport. The phenomenon is a direct consequence of the intrinsic asymmetry of the phase space. The tokamap, thus, can be thought as an application of Hamiltonian ratchets.

IV. INTERPRETATION BY THE SUM RULE

To understand why particles of the stochastic sea display the directed current $\overline{v_\theta}$, we now examine the regular sets of the tokamap's phase space. The following calculations are based on the sum rule which has been derived in Ref. [20]. In systems with a mixed phase space the sum rule requires chaotic transport to compensate for the directed transport occurring in regular phase space regions. The mean chaotic velocity is generally defined as the phase space integral extending over the whole chaotic sea. It can be reformulated such that the chaotic mean velocity follows in terms of regular trajectories only. According to [19,20], transport is an additive quantity of disjoint invariant sets, which leads to the following expression for the velocity of the chaotic sea

$$\overline{v_\theta} = \frac{\mathcal{T}_{layer} - \sum_i A_i \omega_i}{A_{layer} - \sum_i A_i}. \quad (17)$$

Here, A_i is the area of island chain i, ω_i is its winding number, and A_{layer} is the area of the layer. $\mathcal{T}_{layer}$ is the total transport of the layer bounded from below and above by two KAM tori given by

$$\mathcal{T}_{layer} = \int_0^1 d\theta \int_{\psi_u(\theta)}^{\psi_l(\theta)} T'(\psi) d\psi = \langle T \rangle_u - \langle T \rangle_l. \quad (18)$$

To evaluate (17), we compute the areas and winding numbers of the main island chains shown in Fig. 2(a). The values are displayed in Table I.

The area of the layer is $A_{layer} = 0.714 \pm 0.01$.

After finding the upper and lower bounding KAM tori, we calculate, by interpolation, $\psi_u(\theta)$ and $\psi_l(\theta)$, with $\theta = [0,1]$ (uniformly spaced). The kinetic energy of the tokamap is given by Eq. (6) (see also Appendix A). From where we obtain $\langle T(\psi_u) \rangle$ and $\langle T(\psi_l) \rangle$, which inserted in Eq. (18) yields: $\mathcal{T}_{layer} = 0.347 \pm 0.005$.

TABLE I. Areas and winding numbers corresponding to the phase portrait of the tokamap shown in Fig. 2(a).

Island chain	Area	Winding number
1	0.012 ± 0.001	2/7
2	0.002 ± 0.001	3/10
3	0.050 ± 0.002	1/3
4	0.003 ± 0.001	2/5
5	0.063 ± 0.002	1/2
6	0.001 ± 0.001	3/5
7	0.013 ± 0.001	2/3
8	0.001 ± 0.001	5/7
9	0.010 ± 0.002	3/4

Using this result in Eq. (17), we finally arrive at:

$$\overline{v_\theta} = 0.49 \pm 0.01, \quad (19)$$

which is in good agreement with the value found in Sec. III, where $\overline{v_\theta} = 0.50 \pm 0.02$.

The average poloidal velocity $\overline{v_\theta}$ is, therefore, described in terms of regular sets of the phase space. The contribution of each island chain is proportional to its area. The major contribution, however, comes from the total transport, given by the KAM tori.

V. PLASMA ROTATION

The presence of a directed poloidal velocity has interesting physical implications. In what follows, we calculate the velocity distribution of counterpassing particles as well and discuss the consequences of the results.

The phase space of the backward tokamap is depicted in Fig. 4(a) for $L = 4.5/2\pi$. There are some clear observable changes as compared to the forward tokamap. The first is rather obvious: Transport now goes in the opposite direction. The other-less evident is that the areas of regular islands, and also of the entire bounded layer, are now slightly larger (Table II).

The area of the layer is now $A_{layer} = 0.80 \pm 0.01$. Using this result in Eqs. (17) and (18), we finally arrive at

$$\overline{v_\theta} = -0.47 \pm 0.01, \quad (20)$$

which agrees well with the numerical simulation, where $\overline{v_\theta} \approx -0.474 \pm 0.003$.

Particles that follow magnetic-field lines can be divided in two groups: the copassing and the counterpassing ones. The latter group is described by the backward tokamap, while copassing particles follow the forward tokamap. Summing the averaged chaotic velocities of both, we find that a nonzero difference between their values exists. This variation corresponds to a poloidal rotation and is due to magnetic perturbations.

VI. SUMMARY AND CONCLUSIONS

In this paper we have investigated poloidal transport in the tokamap. The latter is a simple model for the zeroth-
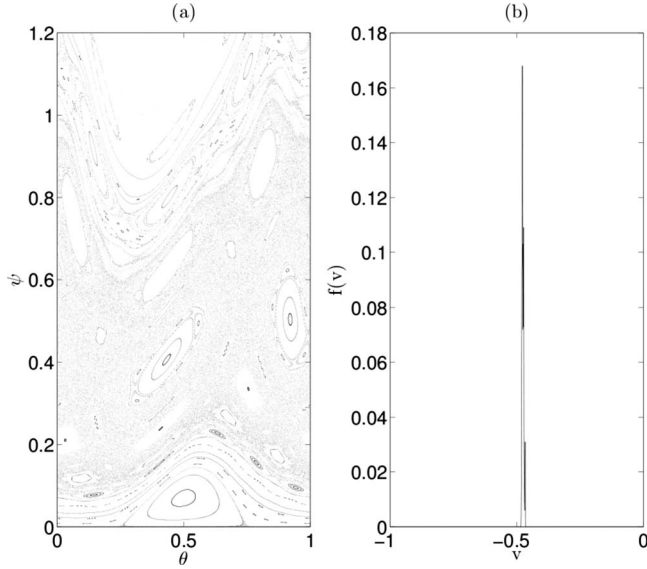
FIG. 4. (a) Phase space of the backward tokamap for L $=4.5/2\pi$. (b) Distribution of time-averaged velocities at time t $\sim 4\times 10^6$. As $t\rightarrow\infty$ it evolves to a narrow peak around the asymptotic velocity, $\overline{v_\theta}\approx -0.474\pm 0.003$.

order guiding-center particle motion in a magnetically confined plasma under the influence of external magnetic perturbations.

First, we showed that the poloidal motion in the (forward) tokamap evolves as a ballistic transport with a narrow velocity distribution. According to the definition proposed in [20] this behavior can be regarded as a Hamiltonian ratchet and follows from the asymmetry of the regular sets of the phase space. We obtained the directed current numerically and compared it with theoretical predictions based on the so-called sum rule, finding an excellent agreement between both. Next, we performed similar simulations for the backward tokamap. The absolute value of the ratchet current, with the same control parameter value, is different from the forward tokamap. This is due to changes in the phase space structure, namely, the increase in the area of regular sets for the backward map.

The presence of a directed current and its connection to phase space structures have major physical implications.

TABLE II. Areas and winding numbers corresponding to the phase portrait of the backward tokamap shown in Fig. 4(a).

Island chain	Area	Winding number
1	0.015 ± 0.001	$-2/7$
2	0.004 ± 0.001	$-3/10$
3	0.056 ± 0.001	$-1/3$
4	0.006 ± 0.001	$-2/5$
5	0.064 ± 0.002	$-1/2$
6	0.002 ± 0.001	$-3/5$
7	0.016 ± 0.002	$-2/3$
8	0.001 ± 0.002	$-5/7$
9	0.012 ± 0.001	$-3/4$
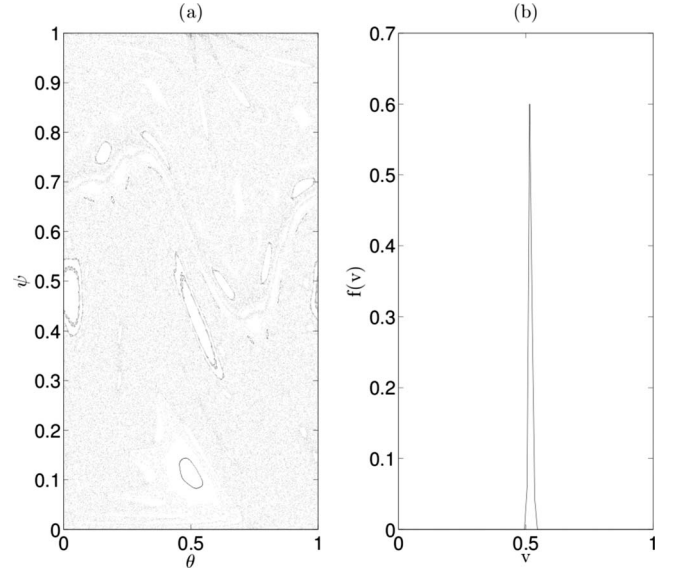
FIG. 5. (a) Phase space of the bounded tokamap for $L=8/2\pi$. (b) Distribution of time-averaged velocities at time $t\sim 4\times 10^6$ for the bounded tokamap.

Typically, magnetic fusion plasmas show a mixed phase space. By considering, as a simple approximation, that particles move along magnetic field lines (copassing and counterpassing), we demonstrated that the appearance of a net poloidal plasma rotation due to a asymmetrical phase space is possible. Finally, we note that, in order to obtain accurate quantitative conclusions, a more complete treatment should be performed with, for instance, more sophisticated Poincaré plots already available for various tokamaks. We stress, however, that the qualitative behavior must remain, since the disparities in drift sections for copassing and counterpassing particles are well known.

The differences in the Poincare sections for the group of particle are generic. For example, the disparities in drift sections for copassing and counterpassing particles are well known. In this paper, the asymmetry is taken into account by the forward and backward tokamap, respectively. The appearance of a net poloidal plasma rotation due to the phase space is demonstrated. This allegories the frequently observed onset of poloidal plasma rotation velocity. Since the sum rule can be easily applied to more sophisticated Poincare plots being available to various tokamaks, the procedures outlined here potentially are useful for even quantita-

TABLE III. Area and winding number for the bounded tokamap as shown in Fig. 5.

Island chain	Area	Winding number
1	0.0142 ± 0.001	$1/1$
2	0.0221 ± 0.002	$1/2$
3	0.0076 ± 0.001	$3/7$
4	0.0126 ± 0.001	$2/5$
5	0.0005 ± 0.001	$3/8$
6	0.0154 ± 0.001	$1/3$

tively correct predictions of rotation velocities in tokamaks with ergodized edges.

APPENDIX A: FURTHER REMARKS ON THE TOKAMAP

It should be emphasized that the tokamap has *not* been rigorously derived from a continuous Hamiltonian system. It was supposed [53] that the tokamap corresponds to the Hamiltonian

$$H = H_0(\psi) + \varepsilon H_1(\psi, \vartheta; \varphi)$$
$$= \int \frac{d\psi}{q(\psi)} - 2\pi L_c \frac{\psi}{1+\psi} \cos(\vartheta) \sum_{k=-\infty}^{\infty} \delta(\varphi - 2\pi k). \tag{A1}$$

From here we define the "kinetic" energy of the tokamap as given by Eq. (6).

A derivation of the tokamap from Hamiltonian (A1) encounters a difficulty related with the presence of delta functions (see [36] and references therein). A regularization procedure has been proposed in Ref. [36]. Because of the Poisson summation formula

$$\sum_{n=-\infty}^{\infty} \cos(n\varphi) = 2\pi \sum_{k=-\infty}^{\infty} \delta(\varphi - 2\pi k), \tag{A2}$$

we may consider

$$H = H_0(\psi) + \varepsilon H_1(\psi, \vartheta; \varphi)$$
$$= \int \frac{d\psi}{q(\psi)} - L_c \frac{\psi}{1+\psi} \cos(\vartheta) \sum_{s=-M}^{M} \cos(s\varphi), \tag{A3}$$

containing the sum of a finite number M of trigonometric functions. It is easy to see that Hamiltonian (A1) follows from the regularized Hamiltonian (A3) in the limit $M \to \infty$. Applying the construction of canonical mappings developed in Refs. [33,53] to Hamiltonian (A3), and performing the limit $M \to \infty$, one can derive the *symmetric tokamap*.

Performing a "trivial" one-step integration in φ over a distance 2π relates the canonical equations based on Eq. (A1) to the tokamap with the identification

$$2\pi L_c \triangleq L. \tag{A4}$$

APPENDIX B: DISTRIBUTIONS IN THE BOUNDED TOKAMAP

It can be rather difficult to localize the exact KAM tori that limit the chaotic layer. To overcome this uncertainty, we now consider the bounded tokamap. With the bounded tokamap, the plasma boundary cannot be crossed.

To ensure $\psi_k > 0$ as well as $\psi_k \leq 1$ we use [6,37]

$$F_0 = F_0|_{\text{tokamap}}, \quad \delta F = -\psi_{k+1}(1 - \psi_{k+1})\cos(\vartheta_k), \tag{B1}$$

to obtain the so-called *bounded* tokamap [6,37]

$$\psi_k = \psi_{k+1} + L\psi_{k+1}(1 - \psi_{k+1})\sin(\vartheta_k), \tag{B2}$$

$$\vartheta_{k+1} = \vartheta_k + 2\pi\Omega(\psi_{k+1}) - L(1 - 2\psi_{k+1})\cos(\vartheta_k). \tag{B3}$$

Introducing $D = L \sin\vartheta_k$, the first Eq. (B2) of the bounded tokamap will be evaluated according to

$$\psi_{k+1} = \begin{cases} \psi_k \dfrac{2}{1 + D + \sqrt{(1+D)^2 - 4D\psi_k}} & \text{for } D > 0 \\[4mm] 1 - (1 - \psi_k) \dfrac{2}{1 + |D| + \sqrt{(1+|D|)^2 - 4|D|(1-\psi_k)}} & \text{for } D < 0. \end{cases} \tag{B4}$$

Now, the two axes $\psi = 0$ and $\psi = 1$ are globally invariant. The bounded tokamap is an explicit map.

The phase portrait of the map is different from the original one. Parameter L still controls the degree of stochastization. For low values, the stochastic layer is divided by a KAM barrier. At higher values, this barrier ceases to exist. Nonetheless, the phase space remains separated for a long transient time. Once this time is over, particles are able to cross the phase space and visit all island chains. Figure 5(a) shows the phase space of the bounded tokamap for $L = 8/2\pi$.

The transient time also affects the velocity distribution of particles on the stochastic sea. While the phase space remains divided, there are different peaks on the probability

distribution. These peaks merge and gather around $\overline{v_\theta}$ after the transient period is over. Figure 5(b) shows the velocity distribution at $t \sim 4 \times 10^6$.

By using the procedure described in Sec. III, we calculate the velocity distribution of an ensemble of particles in the chaotic sea. Through the phase space we find the values presented in Table III.

The boundaries are now well defined, $\psi_l(\theta) = 0$ and $\psi_u(\theta) = 1$, thus the evaluation of Eq. (6) is straightforward. Inserting the results in Eq. (17) we finally arrive at

$$\overline{v_\theta} = 0.512 \pm 0.005. \tag{B5}$$

That agrees well with the numerical simulation result $\overline{v_\theta} \approx 0.518 \pm 0.01$.

[1] A. H. Boozer, Rev. Mod. Phys. **76**, 1071 (2005).

[2] K. H. Finken, in *Dynamic Ergodic Divertor*, special issue of Fusion Eng. Des. **37**, 335 (1997).

[3] I. Caldas *et al.*, Braz. J. Phys. **32**, 980 (2002).

[4] K. Finken, T. Evans, D. Reiter, K. Spatschek, and W. Suttrop, Nucl. Fusion **48**, 024001 (2008).

[5] R. Balescu, M. Vlad, and F. Spineanu, Phys. Rev. E **58**, 951 (1998).

[6] A. Wingen, K. H. Spatschek, and S. Abdullaev, Contrib. Plasma Phys. **45**, 500 (2005).

[7] J. H. Misguich *et al.*, Ann. Phys. France **28**, 1 (2003).

[8] R. Wittkowski, A. Schelin, and K. Spatschek, Contrib. Plasma Phys. **49**, 55 (2009).

[9] C. Hidalgo, in *Turbulent Transport in Fusion Plasmas: First ITER International Summer School*, AIP Conference Proceedings No. 1013, edited by S. Benkadda (AIP, New York, 2008), p. 240.

[10] C. J. McDevitt, P. H. Diamond, O. D. Gürcan, and T. S. Hahm, Phys. Plasmas **16**, 052302 (2009).

[11] K. Finken *et al.*, Nucl. Fusion **41**, 503 (2001).

[12] R. Wolf *et al.*, Nucl. Fusion **45**, 1700 (2005).

[13] K. Finken *et al.*, Phys. Rev. Lett. **94**, 015003 (2005).

[14] M. Lehnen *et al.*, J. Nucl. Mater. **337-339**, 171 (2005).

[15] C. Busch, *Spektroskopische Untersuchung der Poloidalen Plasmarotation Unter dem Einfluss Statischer und Dynamischer Ergodisierung am Tokamak Textor*, Reihe Energietechnik/ Energy Technology Vol. 50 (Foschungszentrum Jülich, Julich, 2006).

[16] C. Busch *et al.*, 33rd EPS Conference on Plasma Physics (ECA, Rome, 2006), Vol. 30I, p. 2.167.

[17] B. Unterberg *et al.*, J. Nucl. Mater. **363-365**, 698 (2007).

[18] P. Reimann, Phys. Rep. **361**, 57 (2002).

[19] H. Schanz, M.-F. Otto, R. Ketzmerick, and T. Dittrich, Phys. Rev. Lett. **87**, 070601 (2001).

[20] H. Schanz, T. Dittrich, and R. Ketzmerick, Phys. Rev. E **71**, 026228 (2005).

[21] L. Wang, G. Benenti, G. Casati, and B. Li, Phys. Rev. Lett. **99**, 244101 (2007).

[22] S. Flach, O. Yevtushenko, and Y. Zolotaryuk, Phys. Rev. Lett. **84**, 2358 (2000).

[23] L. Cavallasca, R. Artuso, and G. Casati, Phys. Rev. E **75**, 066213 (2007).

[24] P. Jung, J. G. Kissner, and P. Hänggi, Phys. Rev. Lett. **76**, 3436 (1996).

[25] J. L. Mateos, Phys. Rev. Lett. **84**, 258 (2000).

[26] S. Denisov and S. Flach, Phys. Rev. E **64**, 056236 (2001).

[27] T. Dittrich, R. Ketzmerick, M. Otto, and H. Schanz, Ann.

Phys. **9**, 755 (2000).

[28] J. Mateos, Physica D **168-169**, 205 (2002).

[29] J. Gong and P. Brumer, Phys. Rev. E **70**, 016202 (2004).

[30] N. A. C. Hutchings, M. R. Isherwood, T. Jonckheere, and T. S. Monteiro, Phys. Rev. E **70**, 036205 (2004).

[31] R. Salgado-García, M. Aldana, and G. Martínez-Mekler, Phys. Rev. Lett. **96**, 134101 (2006).

[32] R. D. Astumian and P. Hänggi, Phys. Today **55**(11), 33 (2002).

[33] I. Y. Dodin and N. J. Fisch, Phys. Rev. E **72**, 046602 (2005).

[34] M. Vlad, F. Spineanu, and S. Benkadda, Phys. Rev. Lett. **96**, 085001 (2006).

[35] M. Vlad, F. Spineanu, and S. Benkadda, Phys. Plasmas **15**, 032306 (2008).

[36] S. S. Abdullaev, Nucl. Fusion **44**, S12 (2004).

[37] M. Eberhard, Phys. Rev. E **71**, 026411 (2005).

[38] V. Kuzovkov and O. Dumbrajs, Compute. Modell. New Technol. **11**, 18 (2007).

[39] V. Kuzovkov and O. Dumbrajs, Physics AUC **17**, 86 (2007).

[40] K. H. Finken *et al.*, *The Structure of Magnetic Field in the TEXTOR-DED, Energy Technology* (Forschungszentrum Jülich, Jülich, 2005), Vol. 45.

[41] S. Abdullaev, Lecture Notes in Physics (Springer, Berlin, 2006) Vol. 691.

[42] A. Wingen and K. H. Spatschek, Phys. Rev. Lett. **102**, 185002 (2009).

[43] A. Wingen, T. Evans, and K. Spatschek, Phys. Plasmas **16**, 042504 (2009).

[44] B. V. Chirikov, Phys. Rep. **52**, 263 (1979).

[45] D. del-Castillo-Negrete, J. M. Greene, and P. J. Morrison, Physica D **91**, 1 (1996).

[46] E. Ott, *Chaos in Dynamical Systems* (Cambridge University Press, Cambridge, 1994).

[47] R. J. Goldston and P. H. Rutherford, *Introduction to Plasma Physics* (Institute of Physics, Philadelphia, 1995).

[48] D. Lesnik and K. H. Spatschek, Phys. Rev. E **64**, 056205 (2001).

[49] B. Weyssow and J. Misguich, 26th Conference on Controlled Fusion and Plasma Physics (ECA, Maastricht, 1999), Vol. 23J, p. 2.59.

[50] D. Constantinescu, Rom. J. Physiol. **50**, 325 (2005).

[51] D. Constantinescu and B. Weyssow, *Order and Chaos in Some Hamiltonian Systems of Interest in Plasma Phyics* (Springer, Berlin, 2006).

[52] M. Eberhard, Europhysics Conference Abstracts, 1999 (unpublished), Vol. 23J, p. 781.

[53] S. Abdullaev, *Construction of Mappings for Hamiltonian Systems and Their Applications* (Springer-Verlag, Berlin, 2006).